

Interlayer Exciton Gases in WSe_2 - pWSe_2 Heterostructures

Zheng Sun,^{*,†} Jonathan Beaumariage,[†] Qingrui Cao,[‡] Kenji Watanabe,[¶] Takashi
Taniguchi,[¶] Benjamin Hunt,[‡] and David W Snoke^{*,†}

[†]*Department of Physics and Astronomy, University of Pittsburgh, Pittsburgh, PA 15260,
USA*

[‡]*Department of Physics, Carnegie Mellon University 15213, USA*

[¶]*Advanced Materials Laboratory, National Institute for Materials Science, Tsukuba, Ibaraki
305-0044, Japan*

E-mail: zhengsun@pitt.edu; snoke@pitt.edu

Phone: +14126249007. Fax: +14126249163

Abstract

The interlayer excitons (IXs) possess a much longer lifetime than direct excitons have been approved owing to the spatial separation of the electrons and holes; hence, they have been pursued to create exciton condensates for decades. The recent emergence of two-dimensional (2D) materials, such as transition metal dichalcogenides (TMDs), and of their van der Waals heterostructures (HSs) (in which two different 2D materials are layered together), has opened new opportunities to study IXs. Here we present the observation of IX gases within two stacked structures consisting of $\text{hBN}/\text{WSe}_2/\text{hBN}/\text{pWSe}_2/\text{hBN}$. The IX energy of the two structures differed by 82 meV, due to the different thickness of the hBN spacer layer between the TMD layers. We demonstrate the lifetime of the IXs is shortened by several folds when the temperature decreases or when

the pump power increases. We attribute the nonlinear behavior of early decay to the Auger process. Our findings give rise to the possibility to design a new generation Quantum well-like TMDs microcavity for exploring the condensation.

Introduction

Interlayer excitons (IXs) (or spatially indirect excitons) are electrons and holes that are bound by Coulomb interaction but spatially separated in two different quantum wells. For decades III-V and II-IV type quantum wells have been investigated as a candidate for IX condensation.¹⁻³ However, the weak binding energy and short lifetime of traditional IXs has hindered that progress.

Transition metal dichalcogenides (TMDs) with the chemical formula of MX_2 ($\text{M} = \text{Mo}, \text{W}; \text{X} = \text{S}, \text{Se}$) recently have attracted intense attention because of their promising potential to be a crucial building block for designing the next generation of spin-, valley-, optical and optoelectrical devices.⁴⁻⁸ Single atomic layer TMDs possess a direct bandgap, extraordinarily strong oscillator strength and larger exciton binding energy than the conventional semiconductors (0.3-0.5 eV).^{9,10} Moreover, the various possibilities of assembling stacks of TMDs via weak van der Waals forces makes them an exciting new platform in investigating light-matter interactions.¹¹⁻¹³ However, optical nonlinearity and the onset of spontaneous coherence has not yet been achieved due to the difficulty of fabricating high Q factor microcavities with a wedge for tunability, resulting in low-density populations and inefficient detunings.

On the other hand, a series of studies about the hetero-bilayers of $\text{MoSe}_2/\text{WSe}_2$ and MoS_2/WS_2 have been reported in the last few years. Ultrafast charge transfer and the formation of interlayer excitons have been demonstrated in photoexcited TMD HSs.^{6,14-17} In particular, the IXs within the HSs exhibit much longer transition and valley depolarization

lifetimes (several hundreds of picoseconds to nanoseconds) compared to conventional semiconductors. The bandgap at the interface of the two different TMDs realigns and forms type II semiconductors eventually. The fixed vertically aligned IX's dipole moment gives rise to the tunability of the IX's energy by applying an out of plane electric field. However, the electrical tunability is limited by the built-in interfacial electric field which produces pristine homobilayer $\text{WSe}_2/\text{WSe}_2$ structures with negligible built-in field.¹⁸ This gives rise to the high electrical tunability of homobilayers IXs. However, a heterostructure with an embedded large index material such as hBN in between the two TMDs has not been studied as thoroughly.¹⁹ The benefit of such a structure could be tuning the thickness of the hBN structure to match the cavity mode's energy to the energy of the IXs, allowing for the observation of many-body nonlinear behavior.

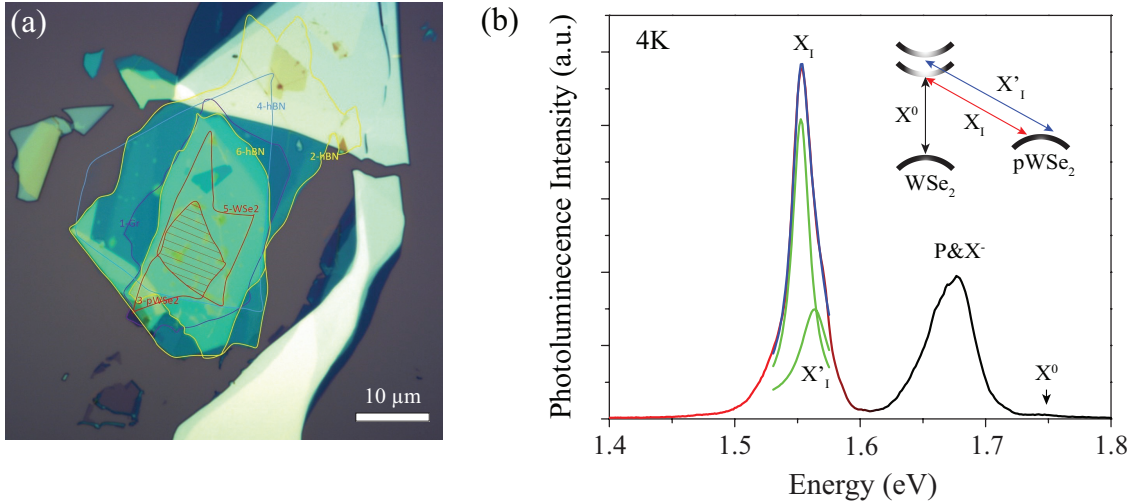


Figure 1: (a) Optical microscope image of interlayer excitons device. The flakes were transferred to a p-doped Si substrate with a top-down method. (d) A typical photoluminescence (PL) spectrum of the heterostructure sample taken at 4 K by He-Ne laser. At cryogenic temperature, the PL from Interlayer excitons and impurities dominate the whole spectrum. A bi-Lorentzian fit is applied to the plot, it determines the XI doublet has energy splitting equal to $\Delta E = 20\text{meV}$. Inset is the illustration of the interlayer excitons transitions in the renormalized bandgap, including the spin levels of the WSe_2 conduction band.

Thus, in this work we fabricated two quantum well-like stacked HSs formed by $\text{hBN}/\text{WSe}_2/$ $\text{hBN}/\text{pWSe}_2/\text{hBN}$ with different hBN thickness for the spacer layer between the two mono-

layers of WSe₂. We present direct observation of interlayer excitons in such type II band structure. We show the IXs energy blueshift as the temperature increases. We find the populations of the doublet for IXs can be modified via tuning the external excitation laser power, a direct illustration of filling up the band energy level from the lower one. Moreover, a kink around 30 K of the integrated intensity ratio of the IXs to intralayer excitons divides the system into two phases. The thermal equilibrium (above 30 K) and non-equilibrium regimes (below 30 K). It indicates that the exciton states are no longer in thermal equilibrium, and/or it may indicate that dark (non-light-emitting) exciton states play a significant role when the temperature is below 30 K. Finally, time-resolved PL measurements give an IX lifetime of ~ 790 ps for sample 1 with the spacer thickness of 2 nm when temperature is below 7 K with excitation power of 0.59 mW. Two decay channels are assigned to the Auger process and exciton recombination. To the best of our knowledge, the Auger effect may not be avoidable in TMD HSs,^{18,20} however inserting a thin layer of large bandgap semiconductor in between the monolayers of WSe₂ could weaken the Auger process without hurting the interaction of the spatially separated electrons and holes. Our method could be applied to other TMD structures to tune the energy of the active medium inside a microcavity.

Results and discussion

Isolated monolayer WSe₂ and pWSe₂ with the typical size of $15 \times 20 \mu\text{m}$ were mechanically exfoliated from bulk crystals purchased from 2D Semiconductors. The two monolayers are encapsulated and separated by the hBN (grown by our collaborators); the whole sandwich structure is in the order of hBN/WSe₂/hBN/pWSe₂/hBN from bottom to top. The whole samples were fabricated by standard dry transferring in a top down method. We made two similar structure samples and one control sample consisting of hBN/WSe₂/hBN. All the samples are with the top and bottom hBN possessing a similar thickness of 15 nm. While the thickness of the hBN spacer layers are 1 and 5 nm, for samples 1 and 2 respectively.

The manuscript shows the data collected from sample 1 with a spacer thickness of 1 nm. The same measurements were performed on sample 2, which showed similar results and is present in the supplementary information.

Figure 1(a) illustrate the design and the optical microscope image of the sample. The p doping of the intrinsic WSe₂ in the HS raises the Fermi level above the valence band, which results in band renormalization and forms a type II semiconductor. This is further confirmed by the photoluminescence (PL) image of the HS which was performed by non-resonantly pumping the device with a 632 nm HeNe laser. The excitation light power is 0.07 mW with a spot size of 5 μ m at normal incidence through a numerical aperture (NA) of 0.75 ($\times 50$) microscope objective (Mitutoyo). The PL signal was collected by the same objective and directed to a grating spectrometer equipped with a charge-coupled device (CCD). All measurements were carried out by cooling the HSs to low temperature (below 10 K) in a continuous-flow cold-finger cryostat. The corresponding spectrum is shown in Fig. 1(b), the distinct spectral feature show IXs at 1.568 eV, while impurities(local excitons) & trions are both at 1.7 eV at cryogenic temperature.^{18,21} A bi-Lorentzian fit applies to the IX peak due to the spin-orbital coupling lift off the degeneracy of the valence band at the K point, and the IX doublet has the energy splitting equal to $\Delta E = \hbar\omega' - \hbar\omega = 20meV$.²²⁻²⁴ The energy splitting agrees well with the theoretical calculation of the conduction band splitting for WSe₂, about 38 meV. In contrast to the other sample with a spacer thickness of 5 nm, the IXs energy here is about 82 meV lower. This is because of the enhanced screening effect due to increasing the thickness of the spacer. Thus, it lowers the IXs binding energy and raises the IXs energy. Inset in Fig.1(b) illustrates the schematic of the lifted off valence band of the WSe₂ and the double transitions channels in HSs.

Next, the temperature-dependent PL was measured under the same configurations. The PL shown in Fig. 2(a) (b) clearly demonstrates the pronounced IX peaks which become

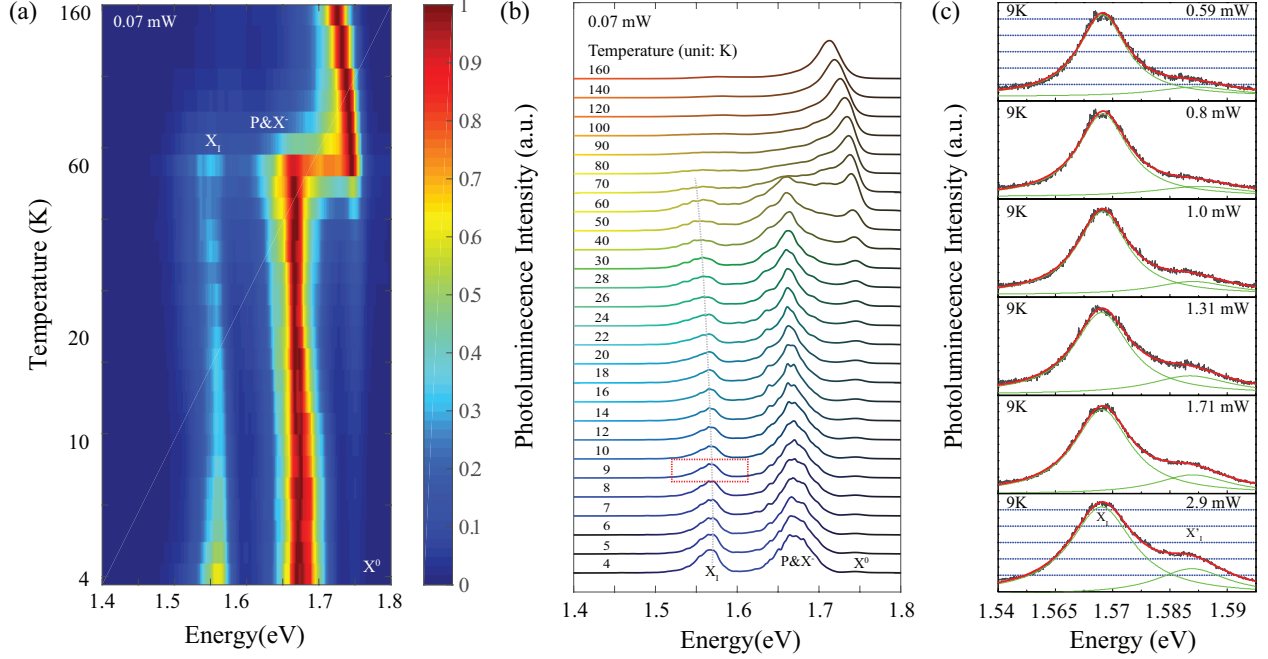


Figure 2: (a) (b) Two different visualizations of temperature-dependent PL created by He-Ne pump laser with excitation power of 0.07 mW. The IXs peak decrease as temperature increases and disappears eventually around 60 K. The dashed gray line indicates the temperature-dependent bandgap shift. (c) Power-dependent photoluminescence of interlayer excitons for at 9 K (peak at 1.568 eV) as boxed (red) in (b) by a mode-locked Ti: sapphire pump laser ($E_{\text{pump}} \approx 1.75\text{eV}$). A bi-Lorentzian fit (green lines) to the plots, normalized for power and integration time. The blue grid lines help to demonstrate the relative intensities of the two peaks, and how they change with temperature. The ratios of the intensity integrated over all energies are $\eta = I_{\omega'}/I_{\omega}$, 7.2% and 19.3% for pump power of 0.59 mW and 2.9 mW respectively.

attenuated as the temperature increases and quenches gradually up to 60 K. The dashed gray line in Fig. 2(b) traces the shift of the exciton energy as a function of the temperature. Power sequence PL of IXs at 9 K as highlighted in the red box in Fig. 2(b) was carried out by a mode-lock Ti: sapphire pump laser ($E_{\text{pump}} \approx 1.75\text{eV}$), shown in Fig. 2(c). A bi-Lorentzian fit was applied to the data (gray line), which was normalized by pump power and charge-coupled device (CCD) integration time. The higher energy and lower energy Lorentzians are shown with the two green lines, and their sum (the red line) agrees well with the data (gray line). The relative intensity of these two sub-peaks changed as we increased the pump power. We define $I_{\omega'}$ as the intensity of the higher energy Lorentzian integrated over all energies,

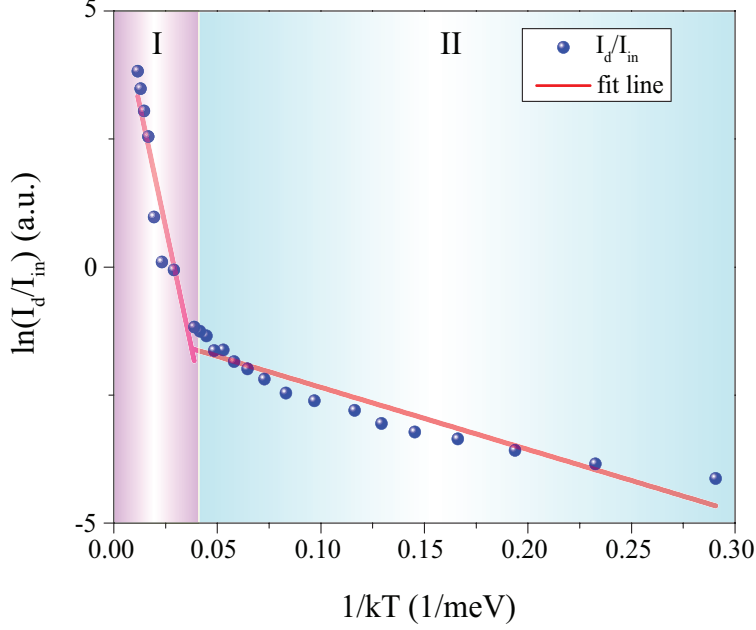


Figure 3: Natural log of the ratio of integrated intensity of the direct and interlayer excitons as a function of $1/kT$, where k is the Boltzmann constant. The colored lines give the results of the fits. The first and second regime, distinguished by background colors, correspond to temperatures above and below 30 K. The fit slope in regime I and II are $-190 \pm 17 \text{ meV}$ and $-12 \pm 1 \text{ meV}$ respectively.

while I_ω corresponds to the lower energy Lorentzian. The ratio of these two integrated quantities, $\eta = I_{\omega'}/I_\omega$, was found to be 7.2% and 19.3% at pump powers of 0.59 mW and 2.9 mW respectively. The IXs are predominantly occupying the lower energy state at lower power until it is close to saturating, at which point the higher energy state begins to fill up. The power dependent blueshift of the IXs has been reported by two other groups,^{14,18} however, it is not seen here because the hBN spacer layer significantly decreased the IX's density. For all tested pump powers, we found the energies of the two sub-peaks to be 1.568 eV and 1.588 eV.

A further analysis was performed to measure the peak intensity of the intralayer and interlayer excitons as a function of the temperature. The result was fitted with the thermal distribution function presented in Fig. 3:

$$\frac{I_d}{I_{in}} = e^{-\frac{\Delta E}{kT}} \quad (1)$$

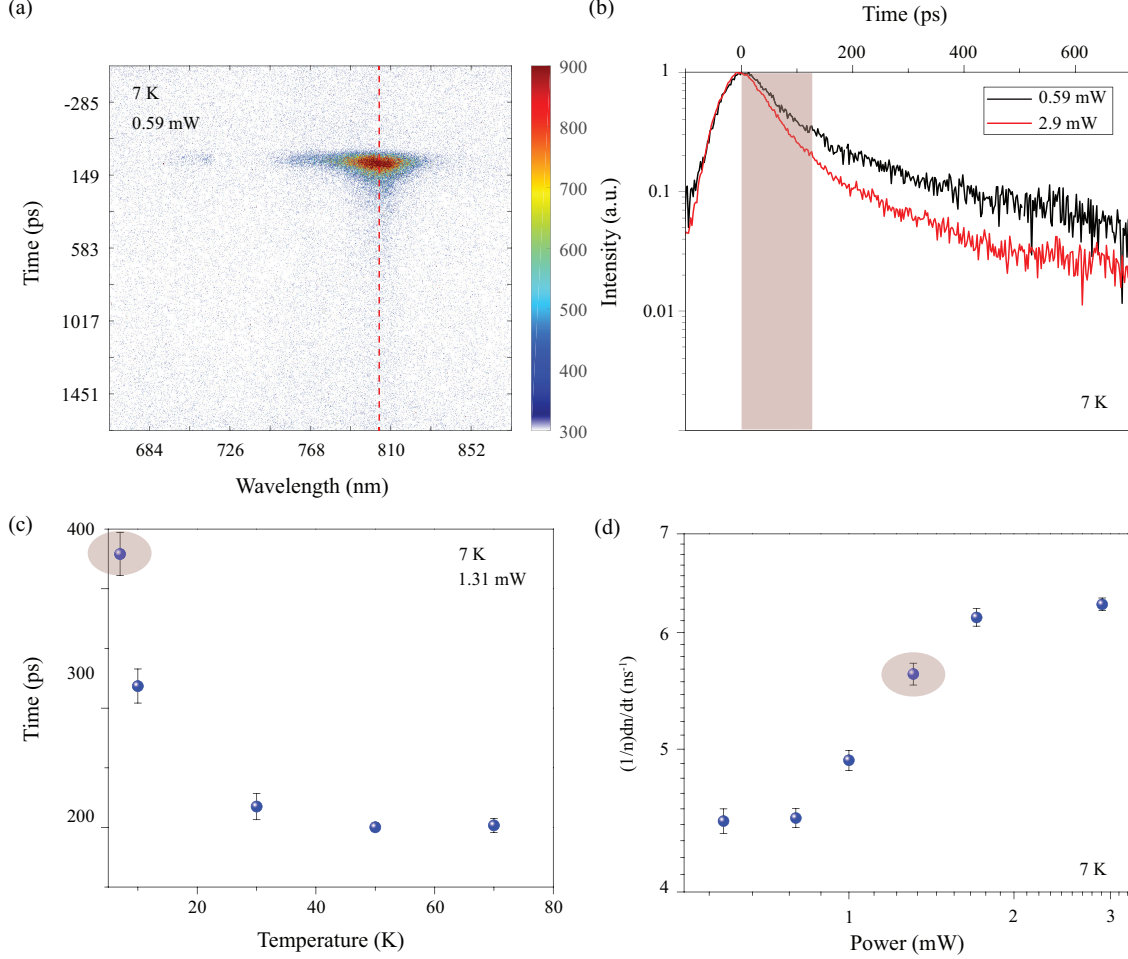


Figure 4: (a) Time-resolved photoluminescence image of HSs (sample 1) measured by streak camera. The interlayer exciton (1.568 eV) shows a lifetime of ~ 790 ps under excitation power of 0.59 mW at 7 K. (b) Lifetime measurements are plotted together under two different excitation power 0.59 mW and 2.9 mW at 7 K. (c) Temperature dependent lifetime of the IXs, with pump power 1.31 mW. (d) Decay rate as the function of the pump power plotted on a log scale measured at 7 K. Highlighted spots in (c)(d) are performed under the same configurations.

I_d and I_{in} are the peak intensity of direct (intralayer) and indirect (interlayer) excitons, k is the Boltzmann constant. We can use this equation to solve for the energy difference between the two states, ΔE . Two distinct regimes are shown separated by a kink around 30 K when we plot the natural log of the relative intensity as a function of $1/kT$ in Fig 3. Fitting the data with a line in regime I, which corresponds to a temperature above 30 K, gives $\Delta E = 190 \pm 17 meV$. This same fitting procedure in regime II (below 30 K) gives $\Delta E = 12 \pm 1 meV$. At 100 K, we find an energy separation of 193 meV, in good agreement

with the prediction of our thermal distribution. However, at 9 K we found an energy separation of 182 meV, much larger than the predicted 12 meV. This may indicate that the exciton states are no longer in thermal equilibrium, and/or it may indicate that dark (non-light-emitting) exciton states play a significant role in thermalization below 30 K. This is plausible as dark excitons have been observed at cryogenic temperatures.²⁵

Time-resolved PL measurements were performed using a Hamamatsu streak camera with a temporal resolution of ~ 1 ps, mounted on an exit port of a 0.5m spectrometer equipped with a 50 grooves/mm reflective grating. A mode-locked pulsed Ti: sapphire laser set to wavelength 711 nm ($E_{\text{pump}} \approx 1.75\text{eV}$) was used for pumping the HSs. A 750 nm long-pass filter was placed in the signal's path to block the pump laser. Fig. 4(a) shows the wavelength-resolved streaked image, with calibrated time axis, the red dotted line is centered on the IXs, around 790 nm. The typical time-resolved PL spectrum plotted on a log scale taken at 7 K under two different pump powers, 0.59 mW and 2.9 mW respectively. The early time curvature with the late time tail of the photoluminescence hints that the decay process of the IXs is non-trivial. The decay rate equation for the IX density is governed by two terms:

$$\frac{1}{n} \frac{dn}{dt} = -An - \frac{1}{\tau}, \quad (2)$$

Here, n is the IX's density, τ is the lifetime and A is the Auger coefficient. The first term on the right side of the equation is the nonlinear decay process which can be attributed to Auger recombination, which dominates at early times. The second term describes the IXs recombination, which dominates at late times. The lifetime for the IXs at 7 K under excitation power of 0.59 mW was found to be ~ 790 ps by linearly fitting the tail in Fig 4(a). The lifetime of the IXs as a function of temperature is shown in Fig. 4(c), and can be fit by an exponential function. This behavior can be explained as the number of the hot phonons assisting in the recombination of the IXs grow exponentially with temperature. Fig. 4(b)

shows the lifetime of the IXs under two different excitation powers, 0.59 mW and 2.9 mW respectively. The increase in power strengthens the interaction between the IXs significantly and results in nearly doubling the decay rate from 1.25 ns^{-1} up to 2.6 ns^{-1} .

The decay process on sample 2 shows similar behavior (see supplementary) with a measured lifetime of 575 ps under excitation power of 0.93 mW. The reason for the shorter lifetime observed in sample 2 is due to the larger spatial separation. The increased space may lower the possibility of recombination or open other decay channels for the IXs, hence shortening the lifetime.

In this paper, we have shown that interlayer excitons can be observed in a vertical stacked structure of hBN/WSe₂/hBN/pWSe₂/hBN, which is similar to a quantum well. The photoluminescence of the IXs is fit by a bi-Lorentzian, showing two IX states with different energies. Due to lower population density, the power dependent blue shifting of these states was not observed, however as the excitation power was increased we observed the lower energy state saturate and the higher energy state begin to fill up. The intensity ratio of the IXs and intralayer excitons follows the standard thermal distribution when the system is above 30 K. However, below 30 K there is a large discrepancy, leading us to believe the dark excitons play a significant role in low temperature thermalization. This agrees with the theoretical calculation of the band structure of WSe₂ showing that the dark excitons possess lower energy states.²²⁻²⁴ The IX's energy shown here is about 1.568 eV measured at 10 K, comparable to the exciton energy in GaAs quantum wells. Thus, it indicates the possibility of creating a new kind of AlGaAs microcavity structure by replacing the traditional GaAs quantum wells with TMD based HSs as the active medium. Additionally, we show the lifetime of the IXs can be significantly affected by the temperature and the excitation power. The exciton decay process is described by a typical rate equation with an Auger process, which the hBN spacer layer did not seem to prevent. Finally, we find the

IXs are quite sensitive to the thickness of the spacer. In contrast to the sample with a 1 nm spacer, the IXs inside the sample with a 5 nm spacer have an energy which has been lifted up to 1.65 eV (see supplementary), an 82 meV blue shift. Our results may have implications for the search of IX condensation and new optoelectronics applications in 2D semiconductors.

Acknowledgement

This work was supported by the US Army Research Office under MURI award W911NF-17-1-0312. The authors declare no competing interests.

Supporting Information Available

The following files are available free of charge.

- Filename: Supplementary Information

References

- (1) Butov, L. V.; Zrenner, A.; Boehm, G.; Weimann, G. Condensation of indirect excitons in coupled AlAs/GaAs quantum wells. *Physical Review Letters* **1993**, *3*, 167–170.
- (2) Butov, L.; Filin, A. Anomalous transport and luminescence of indirect excitons in AlAs/GaAs coupled quantum wells as evidence for exciton condensation. *Physical Review B* **1998**, *58*, 1980–2000.
- (3) Butov, L. V.; Lai, C. W.; Ivanov, A. L.; Gossard, A. C.; Chemla, D. S. Towards Bose-Einstein condensation of excitons in potential traps. *Nature* **2002**, *417*, 47–52.

- (4) Ross, J. S.; Klement, P.; Jones, A. M.; Ghimire, N. J.; Yan, J.; Mandrus, D. G.; Taniguchi, T.; Watanabe, K.; Kitamura, K.; Yao, W.; Cobden, D. H.; Xu, X. Electrically tunable excitonic light-emitting diodes based on monolayer WSe₂ p-n junctions. *Nature Nanotechnology* **2014**, *9*, 268–272.
- (5) Koperski, M.; Nogajewski, K.; Arora, A.; Cherkez, V.; Mallet, P.; Veuillen, J. Y.; Marcus, J.; Kossacki, P.; Potemski, M. Single photon emitters in exfoliated WSe₂ structures. *Nature Nanotechnology* **2015**, *10*, 503–506.
- (6) Schaibley, J. R.; Yu, H.; Clark, G.; Rivera, P.; Ross, J. S.; Seyler, K. L.; Yao, W.; Xu, X. Valleytronics in 2D materials. *Nature Reviews Materials* **2016**, *1*.
- (7) Xu, X.; Yao, W.; Xiao, D.; Heinz, T. F. Spin and pseudospins in layered transition metal dichalcogenides. *Nature Physics* **2014**, *10*, 343–350.
- (8) Lopez-Sanchez, O.; Lembke, D.; Kayci, M.; Radenovic, A.; Kis, A. Ultrasensitive photodetectors based on monolayer MoS₂. *Nature Nanotechnology* **2013**, *8*, 497–501.
- (9) Chernikov, A.; Berkelbach, T. C.; Hill, H. M.; Rigosi, A.; Li, Y.; Aslan, O. B.; Reichman, D. R.; Hybertsen, M. S.; Heinz, T. F. Exciton Binding Energy and Nonhydrogenic Rydberg Series in Monolayer WS₂. *Phys. Rev. Lett.* **2014**, *113*, 076802.
- (10) Ugeda, M. M.; Bradley, A. J.; Shi, S. F.; Da Jornada, F. H.; Zhang, Y.; Qiu, D. Y.; Ruan, W.; Mo, S. K.; Hussain, Z.; Shen, Z. X.; Wang, F.; Louie, S. G.; Crommie, M. F. Giant bandgap renormalization and excitonic effects in a monolayer transition metal dichalcogenide semiconductor. *Nature Materials* **2014**, *13*, 1091–1095.
- (11) Liu, X.; Galfsky, T.; Sun, Z.; Xia, F.; Lin, E. C.; Lee, Y. H.; Kéna-Cohen, S.; Menon, V. M. Strong light-matter coupling in two-dimensional atomic crystals. *Nature Photonics* **2014**, *9*, 30–34.

- (12) Sun, Z.; Gu, J.; Ghazaryan, A.; Shotan, Z.; Considine, C.; Dollar, M.; Chakraborty, B.; Liu, X.; Ghaemi, P.; Kéna-Cohen, S.; Menon, V. Optical control of room-temperature valley polaritons. *Nature Photonics* **2017**, *11*.
- (13) Chakraborty, B.; Gu, J.; Sun, Z.; Khatoniar, M.; Bushati, R.; Boehmke, A. L.; Koots, R.; Menon, V. M. Control of Strong Light-Matter Interaction in Monolayer WS₂ through Electric Field Gating. *Nano Letters* **2018**, *18*, 6455–6460.
- (14) Rivera, P.; Schaibley, J. R.; Jones, A. M.; Ross, J. S.; Wu, S.; Aivazian, G.; Klement, P.; Seyler, K.; Clark, G.; Ghimire, N. J.; Yan, J.; Mandrus, D. G.; Yao, W.; Xu, X. Observation of long-lived interlayer excitons in monolayer MoSe₂-WSe₂ heterostructures. *Nature Communications* **2015**, *6*, 4–9.
- (15) Hong, X.; Kim, J.; Shi, S. F.; Zhang, Y.; Jin, C.; Sun, Y.; Tongay, S.; Wu, J.; Zhang, Y.; Wang, F. Ultrafast charge transfer in atomically thin MoS₂/WS₂ heterostructures. *Nature Nanotechnology* **2014**, *9*, 682–686.
- (16) Rivera, P.; Seyler, K. L.; Yu, H.; Schaibley, J. R.; Yan, J.; Mandrus, D. G.; Yao, W.; Xu, X. Valley-polarized exciton dynamics in a 2D semiconductor heterostructure. *Science* **2016**, *351*, 688–691.
- (17) Lee, C. H.; Lee, G. H.; Van Der Zande, A. M.; Chen, W.; Li, Y.; Han, M.; Cui, X.; Arefe, G.; Nuckolls, C.; Heinz, T. F.; Guo, J.; Hone, J.; Kim, P. Atomically thin p-n junctions with van der Waals heterointerfaces. *Nature Nanotechnology* **2014**, *9*, 676–681.
- (18) Wang, Z.; Chiu, Y. H.; Honz, K.; Mak, K. F.; Shan, J. Electrical Tuning of Interlayer Exciton Gases in WSe₂ Bilayers. *Nano Letters* **2018**, *18*, 137–143.
- (19) Calman, E. V.; Fogler, M. M.; Butov, L. V.; Hu, S.; Mishchenko, A.; Geim, A. K. Indirect excitons in van der Waals heterostructures at room temperature. *Nature Communications* **2018**, *9*, 1–5.

- (20) Sun, D.; Rao, Y.; Reider, G. A.; Chen, G.; You, Y.; Brézin, L.; Harutyunyan, A. R.; Heinz, T. F. Observation of rapid exciton-exciton annihilation in monolayer molybdenum disulfide. *Nano Letters* **2014**, *14*, 5625–5629.
- (21) Yan, T.; Qiao, X.; Liu, X.; Tan, P.; Zhang, X. Photoluminescence properties and exciton dynamics in monolayer WSe₂. *Applied Physics Letters* **2014**, *105*, 101901.
- (22) Liu, G. B.; Shan, W. Y.; Yao, Y.; Yao, W.; Xiao, D. Three-band tight-binding model for monolayers of group-VIB transition metal dichalcogenides. *Physical Review B - Condensed Matter and Materials Physics* **2013**, *88*, 1–10.
- (23) Komider, K.; González, J. W.; Fernández-Rossier, J. Large spin splitting in the conduction band of transition metal dichalcogenide monolayers. *Physical Review B - Condensed Matter and Materials Physics* **2013**, *88*, 1–7.
- (24) Kormányos, A.; Burkard, G.; Gmitra, M.; Fabian, J.; Zólyomi, V.; Drummond, N. D.; Fal, V. Erratum: K·p theory for two-dimensional transition metal dichalcogenide semiconductors (2D Materials (2015) 2 (022001)). *2D Materials* **2015**, *2*, 22001.
- (25) Zhou, Y.; Scuri, G.; Wild, D. S.; High, A. A.; Dibos, A.; Jauregui, L. A.; Shu, C.; De Greve, K.; Pistunova, K.; Joe, A. Y.; Taniguchi, T.; Watanabe, K.; Kim, P.; Lukin, M. D.; Park, H. Probing dark excitons in atomically thin semiconductors via near-field coupling to surface plasmon polaritons. *Nature Nanotechnology* **2017**, *12*, 856–860.